Effect of strontium (Sr) doping on the structural, electronic and optical properties of ZnO, by first-principles calculations

Derkaoui, Issam; Achehboune, Mohamed; Boukhoubza, Issam; El Allam, El mehdi; El Adnani, Zineb; Henrard, Luc; Rezzouk, Abdellah

Published in:
Physica. B: Condensed Matter

DOI:
10.1016/j.physb.2023.414903

Publication date:
2023

Document Version
Early version, also known as pre-print

Effect of strontium (Sr) doping on the structural, electronic and optical properties of ZnO, by first-principles calculations

Issam Derkaoui[1*], Mohamed Achehboune[2], Issam Boukhoubza[1], El mehdi El Allam[1], Zineb El Adnani[3], Luc Henrard[2], Abdellah Rezzouk[1]

[1] Laboratory of Solid state Physics, Faculty of Sciences Dhar el Mahraz, University Sidi Mohammed Ben Abdellah, PO Box 1796 Atlas Fez 30 000, Morocco
[2] Laboratoire de Physique du solide, Namur Institute of Structured Matter, University of Namur, Rue de Bruxelles 61, 5000, Namur, Belgium
[3] Laboratoire d'Ingénierie des Matériaux, de Modélisation et d'Environnement, LIMME, Faculté des Sciences Dhar El Mahraz, Université Sidi Mohammed Ben Abdellah, USMBA, BP 1796 – 30000, Atlas – Fès, Morocco

Corresponding author: derkaouiissam@gmail.com; Tel.: +212-619567896 (I.D.)

Abstract.

We apply the first principles approach using the GGA-PBE+U approximation to study the effect of Sr doping on the structural, electronic and optical properties of ZnO. The computed results show that the optimized lattice parameters as well as the calculated band gaps of pure ZnO and Sr-doped ZnO (SZO) at low and high concentrations are in good agreement with the experimental data. Electronic investigations show that for low Sr concentrations, the appearance of Sr 5s states at a lower energy level than the Zn 4s states at the bottom of the conduction band, causes a reduction of the band gap. However, by increasing further the Sr content, the band gap increases because the Sr 5s states shift to higher energies. The calculated optical properties improve the optical performance of the SZO systems. Hence these findings provide a theoretical reference for future research on Sr-doped ZnO.

Keywords: GGA-PBE+U, SZO, Electronic properties, DFT calculations, Optical properties.

1. Introduction

As a semiconductor with a large direct bandgap of 3.37 eV [1, 2] and a large exciton binding energy of 60 meV at room temperature, zinc oxide (ZnO) has attracted significant interest for its potential applications across optical and optoelectronic devices [3]. Owing to its thermal and chemical stability and efficient excitonic emission, ZnO may prove to be a promising material for several applications, which include light emitting diodes (LEDs) [4] transparent conducting oxides for solar cells [5] transparent thin-film transistors [6] and gas sensors [7, 8]. ZnO also exhibits better efficiency in photocatalytic degradation compared to other metal oxides (e.g., TiO_2) due to its high reactivity [9].

Doping pure ZnO with non-metallic and metallic elements have been considered as a promising way to tune its properties in order to design new ZnO-based devices. For example, Yu et al. have shown that N, C, and S doping represent a potentially promising way to increase the quantum efficiency of ZnO-based photocatalysis [10]. Regarding metal dopants, Ga [11], Al [12], and Fe [13] have been widely studied. Besides, Zhang et al. have calculated the electronic and optical transition of heavy metal doped ZnO, and have demonstrated that Ag or Au doped ZnO enhances the optical transitions [14]. Other investigations show that doping with metal elements increases the excitonic relaxation time, which increases the possibility of their reaction with peripheral ions and therefore enhancing photocatalytic activity [15].

In comparison with transition metal elements, alkaline earth metals dopant can be a suitable choice for ZnO doping due to the absence of d-shell in their electronic structure, which could decrease the threshold energy of absorption [16]. Among them, strontium (Sr) has been used recently with the potential to improve the performance of ZnO for many applications. In particular, the effect of dopant concentrations in Sr-doped ZnO films on love wave filter characteristics has been examined [17]. In addition, it has been demonstrated by Vijayan et al. that SZO films, and especially for higher concentration, deposited with a chemical bath deposition method can have high sensitivity to ethanol vapor with a maximum of 55% [18]. Furthermore, another study [19] has demonstrated that the red shift in band gap enhanced white light luminescence from SZO nanorods, prepared by cost effective reflux method. Likewise, further studies [20, 21] investigate the effect of Sr doping on the optical properties' enhancement of ZnO thin films prepared by spray pyrolysis method. Attempts have been made most recently to obtain SZO nanoparticles, for photocatalytic applications [22, 23]. Beside these experimental studies, there have been very limited theoretical investigation on the structural and electronic properties of SZO.

In a semiconductor material, the electronic band structure is one of the most essential characteristics, because it provides the information about the energy levels of electrons and band gap, allowing the description and understanding of many important properties such as the optoelectronic properties. Therefore, accurate prediction of electronic band structures is very important. First-principles calculations serve as a valuable tool that can help us calculate the electronic structures and optical properties of materials [24-28]. In addition, DFT has become a popular methodology to perform an in-depth analysis of relevant properties of the synthesized nanomaterials at the atomic scale [29-31], as well as to investigate the effect of intrinsic point defects on the electronic and optical properties of semiconductor materials [32, 33].

Herein, for the first time, we systematically investigate numerically the effect of strontium doping of ZnO in the case of low and high concentrations, regarding the evolution of crystal structures, electronic and optical properties with the dopant concentration by means of DFT calculations using GGA-PBE+U approach. The analysis was carried out using low (i.e. 4.17) and high (i.e. 6.25, 8.34, 12.5 and 25 at.%) Sr concentrations. Our refined analysis can provide new insights into the fundamental understanding of the variation of electronic and optical properties of SZO systems, and potentially help to the development of new applications.

2. Computational Method

First-principles calculations were carried out using the Cambridge Serial Total Energy Package (CASTEP). There are based on the density functional theory (DFT) [34] combined with the Perdew-Burke-Ernzerhof generalized gradient approximation (GGA-PBE) [35] by applying the GGA-PBE+U method, where U is an effective on-site interaction parameter. Plane-wave ultra-soft pseudo-potential method [36] with valence electron configurations of $4s^2 3d^{10}$ for Zn, $2s^2 2p^4$ for O, and $4s^2 3d^{10} 4p^6 5s^2$ for Sr was employed to perform the present calculation with a cut-off energy of 420 eV [37]. The Brillouin zone integrations are performed with a Monkhorst-Pack scheme and a grid size of 5×5×4 is used for pure ZnO [38] and 4×4×2 for Sr-doped ZnO

[39]. The convergence threshold for self-consistent iteration was set at 10^{-5} eV/atom, and the lattice parameters and all atomic positions for each supercell were fully relaxed until the maximal force on each atom was less than 0.03 eV/Å, the internal stress was below 0.05 GPa, and the displacement of each atom was below 0.001 Å.

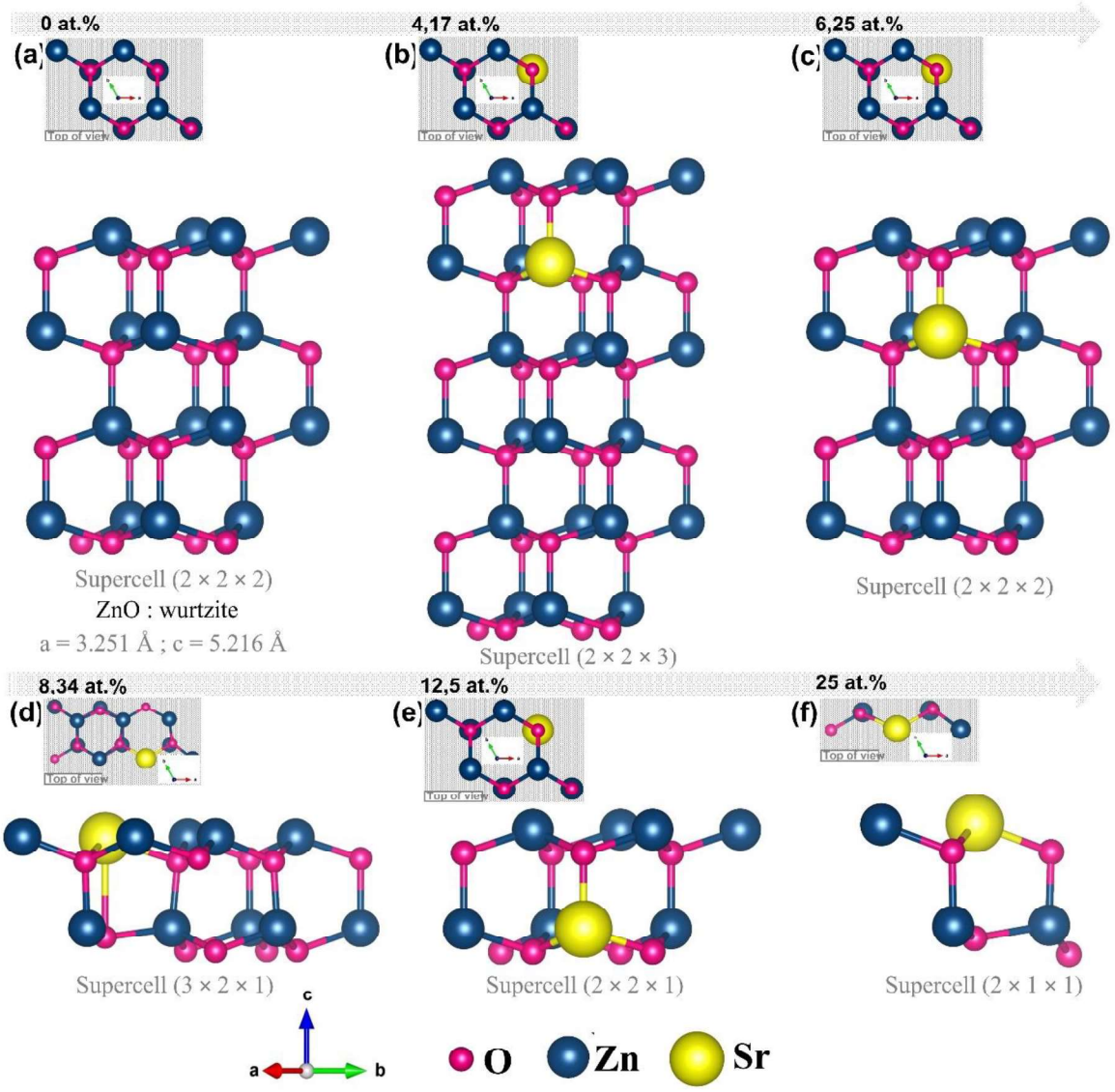

Figure. 1. Schematic of the structure of pure ZnO and SZO systems: (a)- ZnO, (b)- $Zn_{0.9583}Sr_{0.0417}O$, (c)- $Zn_{0.9375}Sr_{0.0625}O$, (d)- $Zn_{0.9166}Sr_{0.0834}O$, (e)- $Zn_{0.875}Sr_{0.125}O$ and (f)- $Zn_{0.75}Sr_{0.25}O$.

We accurately describe the electronic structures by applying the Hubbard U correction to the Zn-3d, O-2p states and Sr-4p. The U_p (O) value of 7 eV for oxidized materials is appropriate for first-principles calculations, according to previous work [40-43]. Therefore, we adopted U_p (O)

= 7 eV, U_d (Zn) = 10 eV and we fix the Hubbard parameter at 2 eV for the Sr-4p electrons in the case of doping. Details regarding band gap variation of pure ZnO with $U_{d,(Zn)}$ are given in the Supporting Information (Figure S1).

Starting from the primitive cell, Figure 1 (a) illustrates a 2×2×2 supercell (with 32 atoms, $Zn_{16}O_{16}$) of pure ZnO, while Figures 1 (b), (c), (d), (e) and (f) illustrate SZO systems from 4.17 ($Zn_{23}Sr_1O_{24}$), 6.25 ($Zn_{15}Sr_1O_{16}$), 8.34 ($Zn_{11}Sr_1O_{12}$), 12.5 ($Zn_7Sr_1O_8$) to 25 at.% ($Zn_3Sr_1O_4$), respectively. In all the supercells shown in Figure 1 as well as for all different concentrations of Sr, a single Sr atom replaces one of the Zn atoms. For Sr-doped ZnO with 4.17 and 6.25 at.%, the composition corresponds to $Zn_{0.9583}Sr_{0.0417}O$ and $Zn_{0.9375}Sr_{0.0625}O$ with a supercell 2×2×3 and 2×2×2, respectively. For 8.34 at.%, the composition corresponds to $Zn_{0.916}Sr_{0.0834}O$, with a supercell 3×2×1, respectively. From 12.5 to 25 at.%, the composition corresponds to $Zn_{0.875}Sr_{0.125}O$ and $Zn_{0.75}Sr_{0.25}O$ with a supercell 2×2×1 and 2×1×1, respectively. In addition, the small pictures in Figure 1 show the increase in Sr concentration from 0 to 25 at.%, taken in the top view.

3. Results and discussion

3.1 Geometry optimization

We carried out an optimization of the equilibrium with the aim of determining the validity of our simulation. The stable phase of ZnO at ambient temperature and pressure is a hexagonal wurtzite (WZ) structure (Space group; P6_3mc). Originally, the primitive cell parameters a = 3.249 Å and c = 5.205 Å ($\alpha = \beta = 90°$ and $\gamma = 120°$) (e.g. ISDD card N°. 5-0664) were used for pure ZnO. A comparison of the optimized lattice parameters, volume, and optical gap energy of pure ZnO with the available experimental and theoretical data are included in the Supporting Information (Table S1). The deviation in lattice parameters between the calculated and standard values was less than 1%, indicating that our calculations after optimization are reliable and proves the validity of our approach.

Table 1. Calculated lattice parameters, volume, Mulliken charges and supercell (K-P) of pure ZnO and SZO systems (4.17 to 25 at.%).

	Lattice parameters			Mulliken charges |e|			Supercell
	a (Å)[a]	c (Å)[a]	V (Å^3)[a]	Zn	Sr	O	K-P
ZnO	3.251	5.216	47.775	0.94	-	-0.94	2× 2 × 2
4.17%	3.277	5.265	48.990	0.93	1.07	-0.94	2× 2 × 3
6.25%	3.288	5.285	49.512	0.92	1.08	-0.94	2× 2 × 2
8.34%	3.301	5.272	49.935	0.91	1.08	-0.95	3× 2 × 1
12.5%	3.341	5.329	51.515	0.91	1.09	-0.94	2× 2 × 1
25%	3.453	5.417	55.371	0.85	1.09	-0.94	2× 1 × 1

[a]: Note that the lattice parameters and volume are normalized.

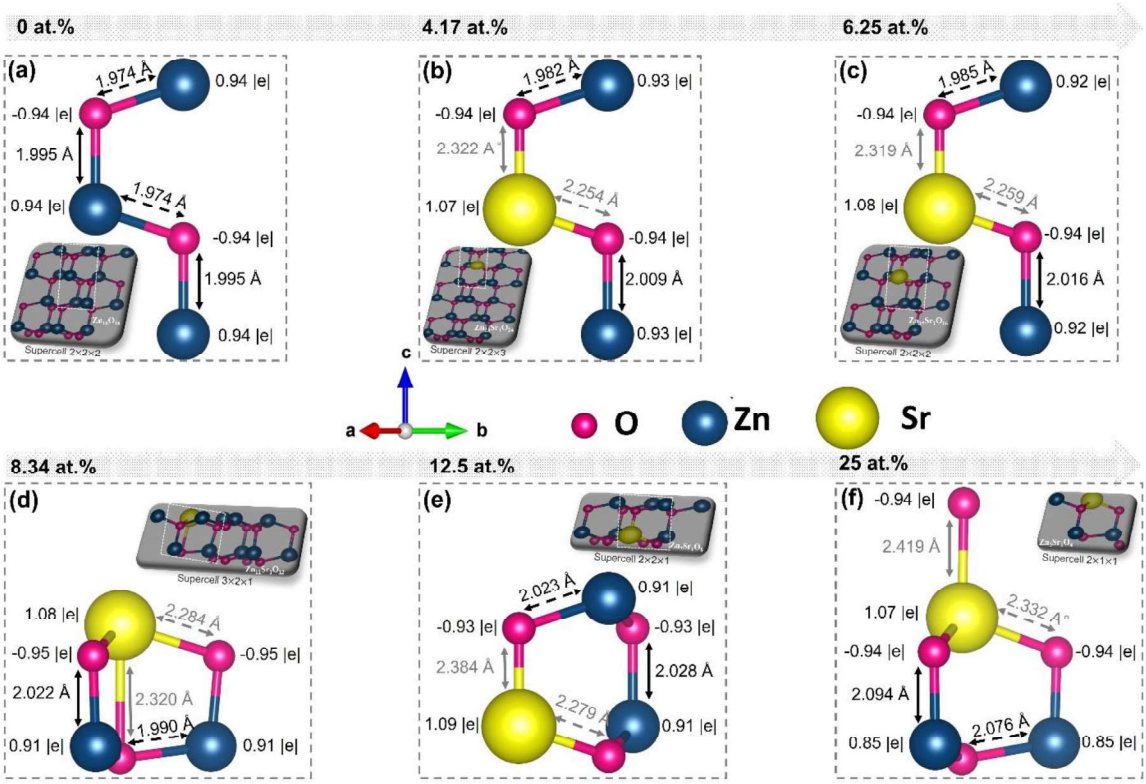

Figure. 2. Bond length and Mulliken charges for the atoms adjacent to the substitutional Sr atom with different concentrations.

The lattice parameters, volume, Mulliken charges and supercell (K-P) of pure ZnO and SZO systems for different dopant concentration (4.17 to 25 at.%) are summarized in Table 1. We observe an increase of the lattice parameters and of the volume with the doping concentration and no change in symmetry observed. This is due to two factors: firstly, the ionic radius of Sr is larger than that of Zn. Secondly, the repulsion between Zn and Sr causes further expansion of the cell. These findings are consistent with the experimental results [1, 20, 22, 23].

Within such a crystal lattice, the Mulliken charges describes the extent of the electron density sheared by an atom compare to neutral atoms. As indicated in Table 1 and Figure 2, the Sr-O bond length is longer than the Zn-O bond length and as the Sr concentration increases, all bond lengths parallel and vertical to the c-axis direction increase compared to pure ZnO. In addition, Mulliken population analysis suggests that Sr has a larger positive charge than Zn (1.09 vs. 0.91 for 12 at.%), while the variation of the Mulliken charges for O is not significant. The Sr dopant contributes more to the oxygen reduction than Zn and the Coulomb attraction between Sr and O (|(1.09)(-0.91)|) is then larger than between Zn and O (|(0.91)(-0.94)|). More information on the average band length/volume as a function of the Sr concentration is given in the Supporting Information (Figure S2).

3.2 Electronic properties

3.2.1 Undoped ZnO

The band structure, the partial density of states (PDOS) and the total density of states (TDOS) of pure ZnO, as shown in Figures 3-4 (a). Meanwhile, Figures 5 and 6 illustrate a schematic of the variation of the band gap and the electronic orbitals distribution evolution in function of Sr concentrations, respectively. According to Figure 3 (a), the calculated electronic band structure shows that pure ZnO is a semiconductor with a direct band gap at Gamma of 3.37 eV, which is in excellent agreement with previously reported experimental values [1, 2]. It should be noted that, in the standard DFT calculations, only an approximate band gap of 0.74 eV can be obtained for pure ZnO. In order to obtain further details about the electronic properties; more specifically, the atomic orbital contributions in the formation of each energy band, we calculated the total (TDOS) and the partial (PDOS) densities of states of pure ZnO (Figure 4 (a)).

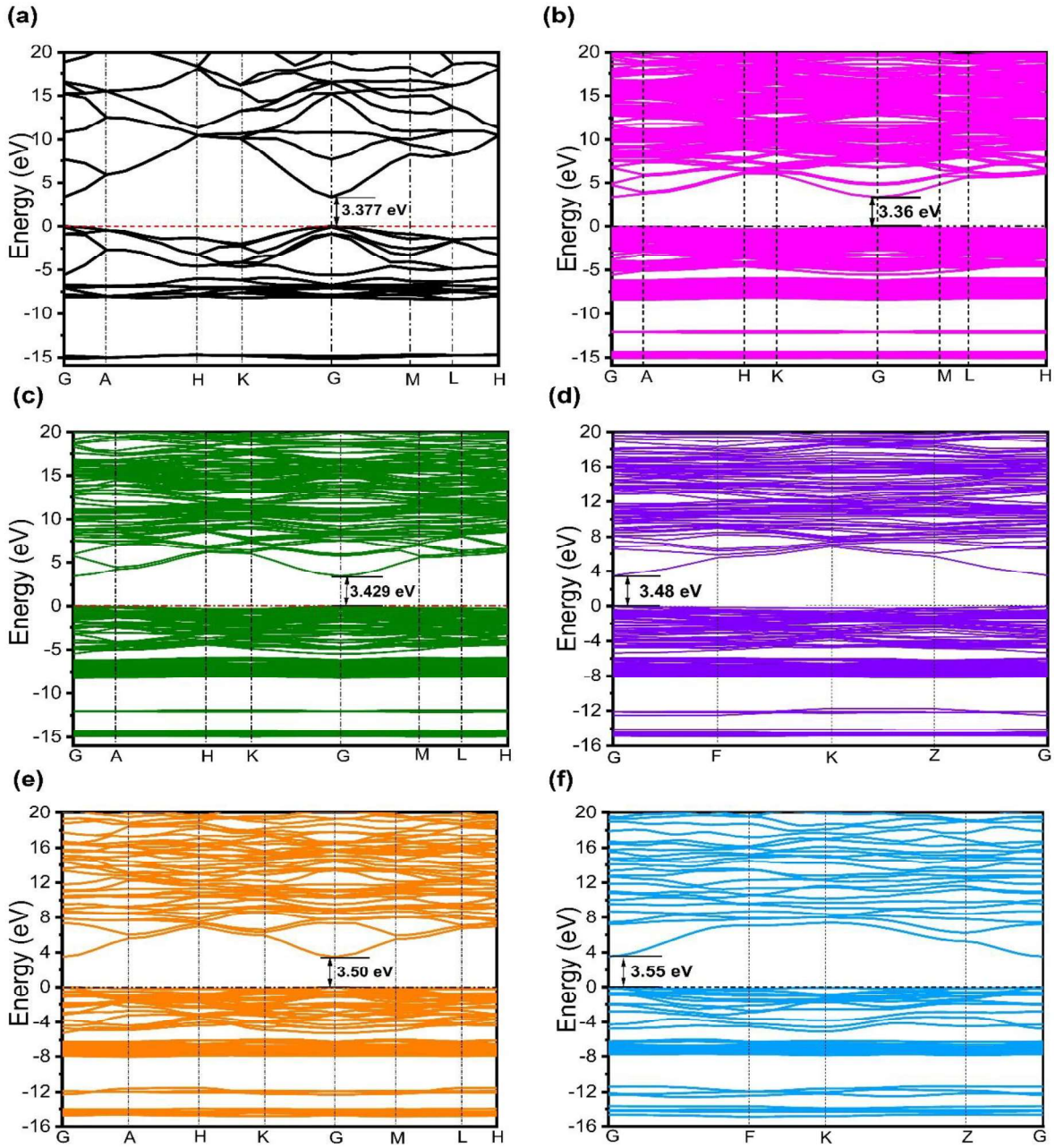

Figure. 3. Band Structure of pure ZnO and SZO systems: (a)- ZnO, (b)- $Zn_{0.9583}Sr_{0.0417}O$, (c)- $Zn_{0.9375}Sr_{0.0625}O$ (d)- $Zn_{0.9166}Sr_{0.0834}O$, (e)- $Zn_{0.8750}Sr_{0.1250}O$ and (f)- $Zn_{0.75}Sr_{0.25}O$. Each band energy is shifted with reference to the Fermi level, being set to zero.

It shows that the valence band (VB) mainly consists of contributions from 2p and 2s states of O, and 3d states of Zn. On the other hand, the conduction band (CB) is mainly composed of the 4s and 4p states of Zn, and the 2p states of O. As we can see from Figure 4 (a), the VB is situated between -15.5 and 0 eV and split into three parts. The upper part (-5.4 eV to 0 eV) of the VB is consists mostly of O 2p states with a minor contribution from the Zn 3d states, resulting in d-p

coupling. While the middle part (-8.8 to -5.4 eV) of the VB is mainly composed of Zn 3d and partial O 2p states. Finally, O 2s states are the main contributors to the bottom part (-15.5 to -13.8 eV) of the VB, with some small contribution from the Zn 3d states. This is described schematically in Figure 6 (a). It has been experimentally reported that the CB is mainly made up of Zn 4s states and 2p states in O-sites [44]. In contrast, our study showed that the composition of the CB is consistent with the total density of ZnO, and mainly formed by Zn 4s and Zn 4p states mixed with a small amount of O 2p states (See Figure 6 (a)). Similar results have also been reported by Wu et al. [40].

3.2.2 Sr-Doped ZnO

We now turn to Sr-doped ZnO. Figures 3 (b-f) illustrate the electronic band structure with varying Sr concentrations in which all concentrations show direct band gaps. From the band structure, we observed that at low Sr concentration (i.e. 4.17 at.%), the conduction band of SZO is slightly shifted downward. These results are in agreement with the experimental results, which show that Sr doping up to 5% causes a decrease of the band gap [20, 23]. Following the substitution of a Zn atom with a Sr atom, both Sr 3d and Sr 5s states appear in the CB, where the minimum of this band is determined by the Sr 5s states. While the Sr 4p states appear in the low energy band (Figure 4 (b)). because of the lower atomic level.

In contrast, for high Sr concentrations (i.e. 6.25, 8.34, 12.5 and 25 at.%), the corresponding band gap values were found to be, 3.42, 3.45, 3. 50, and 3.55 eV, respectively (Figures 3 (c-f) coupled with Figure 5). All these values are higher than those of pure ZnO. These results are in agreement with the experimental and theoretical results [18, 45]. Analyzing the PDOS (Figures 4 (c-f)), we observe that the CB minimum edge is determined by Zn 4s states as for pristine ZnO and shift to higher energy as Sr concentration increased from 6.25 to 25 at.%. The Sr-5s level are displaced to higher energies. Furthermore, the Sr 3d contributes significantly to CB and the Sr 4p states in the VB contribute to the two peaks located at -12 eV and -15 eV. This is schematically

illustrated in Figure 6. The increase in band gap energy at high levels of doping could be assigned to the difference in ionic radius between Sr and Zn. This creates lattice distortion in the lattice structure, which in turn leads to changes in the electronic structure of the material. As a result, localized energy levels may be formed near the conduction band, contributing to the observed increase in band gap as the Sr doping concentration increases.

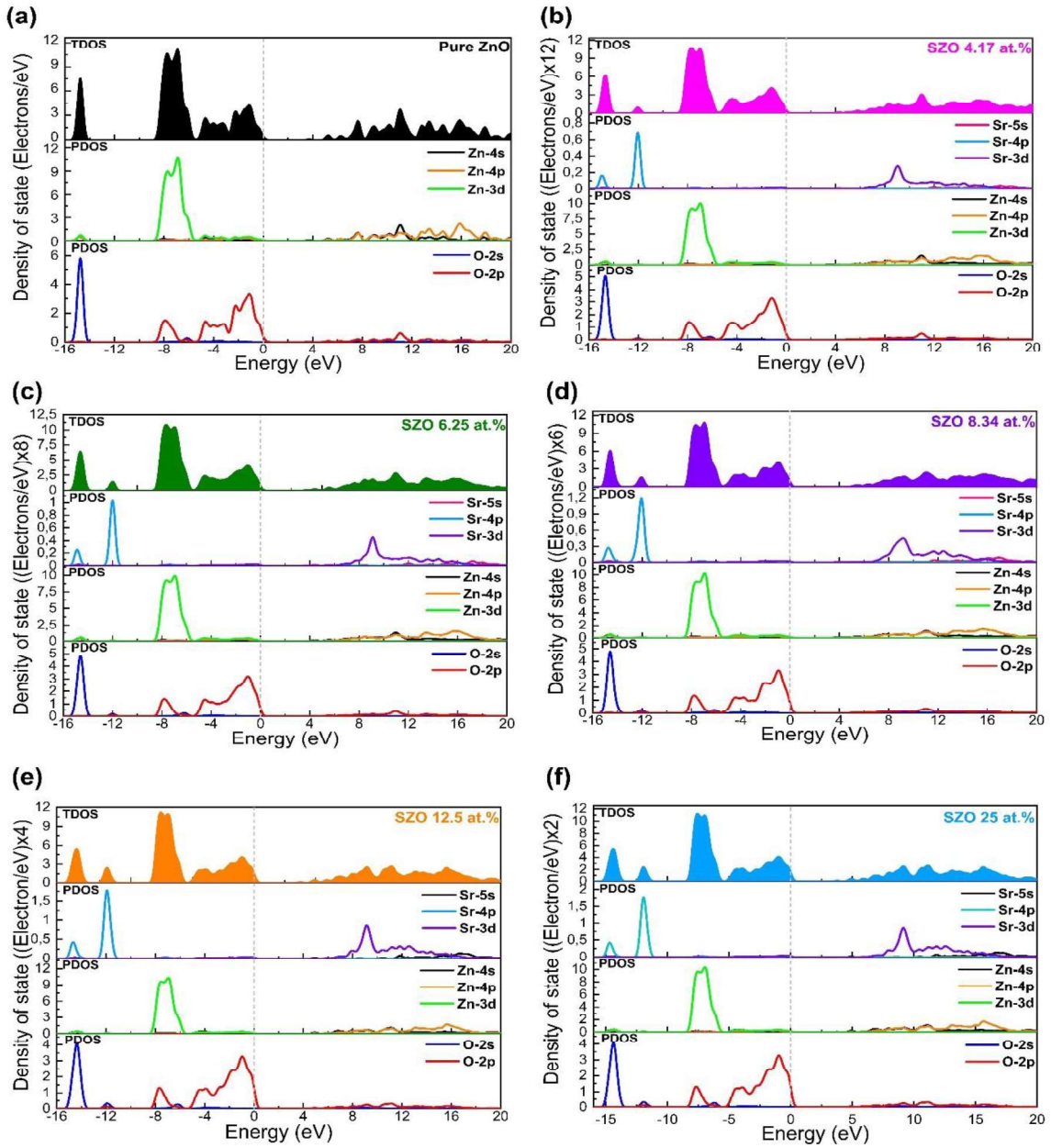

Figure. 4. TDOS and PDOS of pure ZnO and SZO systems, where the Fermi level is set to 0: (a)- ZnO, (b)-$Zn_{0.9583}Sr_{0.0417}O$, (c)- $Zn_{0.9375}Sr_{0.0625}O$, (d)- $Zn_{0.9166}Sr_{0.0834}O$, (e)- $Zn_{0.8750}Sr_{0.1250}O$ and (f)- $Zn_{0.75}Sr_{0.25}O$.

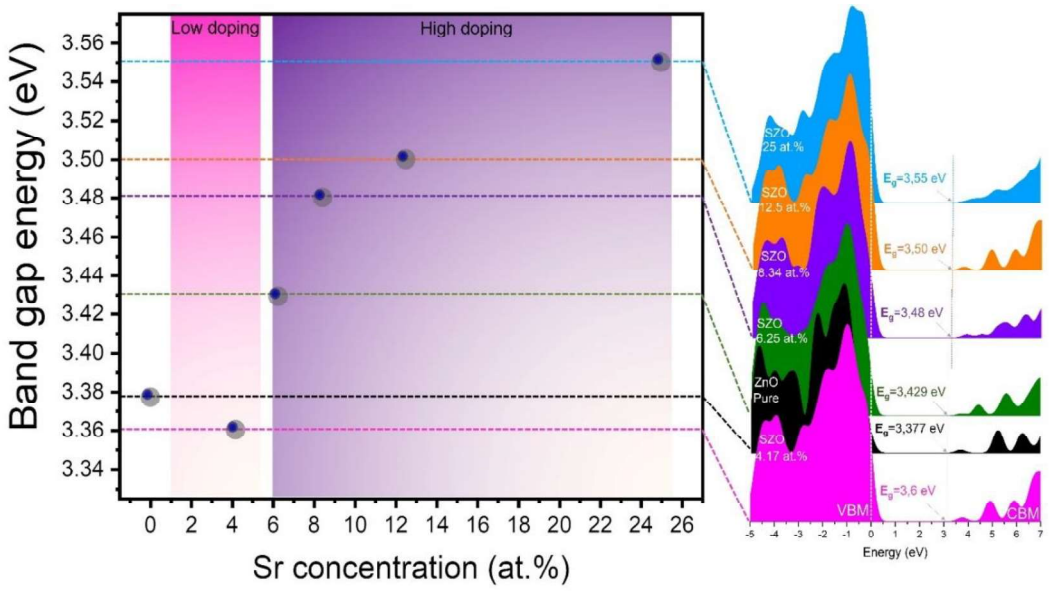

Figure. 5. Schematization of band gap variation in function of Sr concentrations.

Experimentally, in the case of low Sr doping concentration, Raghavendra et al. reported the reduction in the band gap from 3.32 eV in the undoped ZnO to 3.23, 3.21 and 3.17 eV at Sr concentrations of 1, 2 and 3% respectively. They attributed this reduction to the increase in crystallite size [20]. Other observations were also reported by Suwanboon at al. [23], show that the band gap of ZnO was reduced after doping with Sr. This behavior explained by the existence of defects in ZnO lattices, which caused a shift in the absorption band edge to a lounger wavelength, as a result of a reduction in the optical band gap [23].

Several recent experimental and theoretical works show that high Sr doping causes an increase of the band gap [18, 45]. Vijayan et al. [18] have shown experimentally, using UV analysis, that the band gap of ZnO thin films, synthesized by the chemical bath deposition method, increased for high Sr concentration from 3.20 to 3.27 eV. Furthermore, Mahmood et al. [45] theoretically investigate by DFT calculation the effect of Sr doping on the electronic band structure and optical properties of ZnO. They showed an increase in the band gap from 0.76 eV in the undoped ZnO to 0.83 (6 at.%) and 0.92 eV (12 at.%), for one and two Sr-doped atoms, respectively.

We emphasize that in the case of alkaline earth metals (i.e. Sr) the modification of the band gap is related to shape of the CB and the relative energy of the Sr 5s and Zn 4d levels. For other type of dopants, theoretical works [40, 46] have shown the modification of the optical absorption edge in due to the Burstein–Moss effect, i.e. the partial filling of the conduction band by extra-electrons coming from dopant atoms.

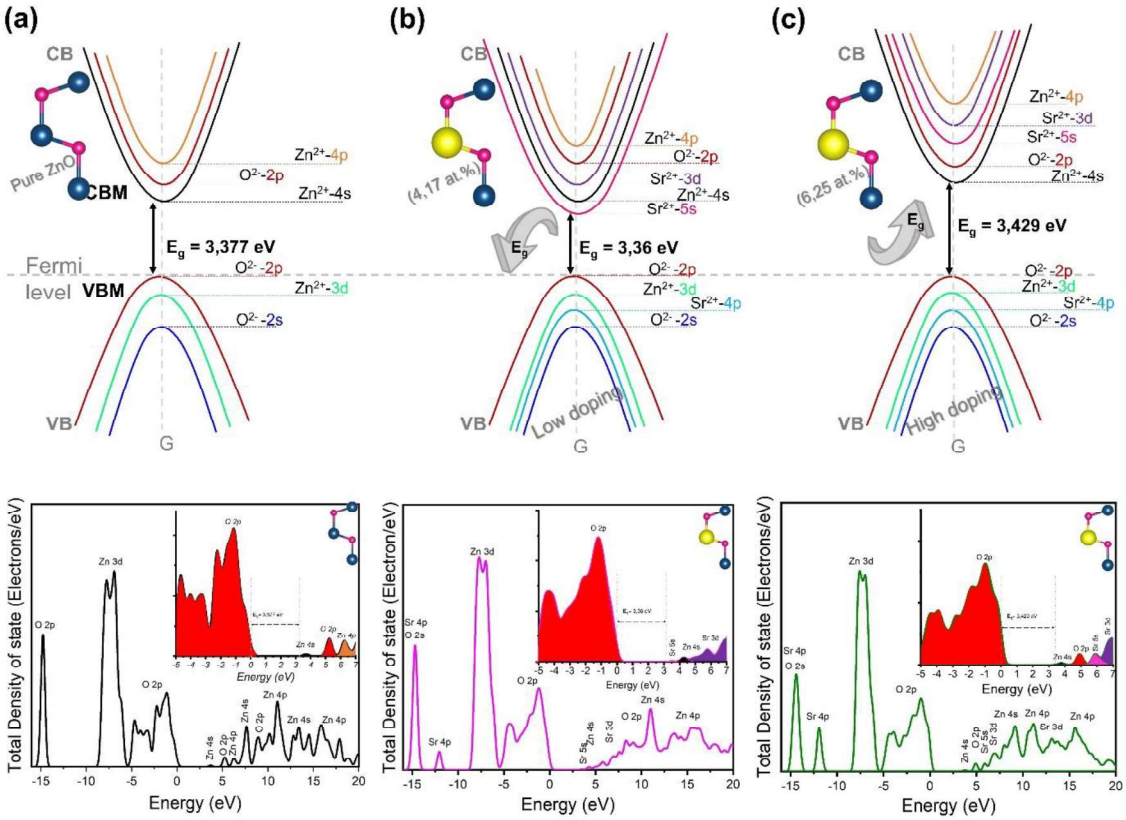

Figure. 6. Schematic of gap energy of (a)- ZnO, (b)- low doping (4.17 at.%; $Zn_{0.9583}Sr_{0.0417}O$) and (c)- high doping (6.25 at.%; $Zn_{0.9375}Sr_{0.0625}O$).

When studying Sr-doped ZnO, it is essential to evaluate the structural, thermodynamic, and dynamical stability [47-52]. This is because studying the physical properties of unstable compounds would not be fruitful. The structural stability of a solid material is determined by the way in which its bonding type and arrangement are reflected by the charge density differences. The graph in Figure 7 illustrates the variations in charge density between undoped ZnO and Sr doped ZnO, in which a higher value (orange regions) represents a gain of electrons. Figures 7 (b-

c) indicates a clear difference in the charge density distribution due to the presence of Sr. This difference is evident in the Mulliken charge values as listed in Table 1, as the electron densities around Zn^{2+} (0.93 e) and Sr^{2+} (1.07 e) ions are dissimilar. When Sr is incorporated into a crystal, the electron density distribution between the ZnO crystal lattice ions is modified, as demonstrated in Figures 7 (b-c). The calculated bond length for the Zn-O bond in Sr-doped ZnO is 2.009 Å, which is larger than that for the corresponding bond in pure ZnO (1.995 Å). Thus, the electronic interaction in ZnO can be changed by the addition of Sr, which leads to Sr-doped ZnO with a larger band gap compared to pure ZnO when the Sr content is above 6.25 at.%. Furthermore, the addition of Sr results in electronic hybridization between the Sr and O atoms, as demonstrated by the formation of the Sr-O bond. Figures 7 (b-c) shows that the calculated bond lengths for the Sr-O bond are longer (2.254 Å and 2.259 Å) than that of the corresponding Zn-O bond (1.974 Å), this gives the existence of ionic bonding, with a slight difference in covalency between the bonds parallel to c-axis and those vertical to it. Furthermore, the results obtained in [45] are in line with the findings of the present study. Therefore, the addition of Sr affects the structural stability of Sr-doped ZnO systems and suggests that it will become more difficult to obtain a high concentration of Sr doped ZnO.

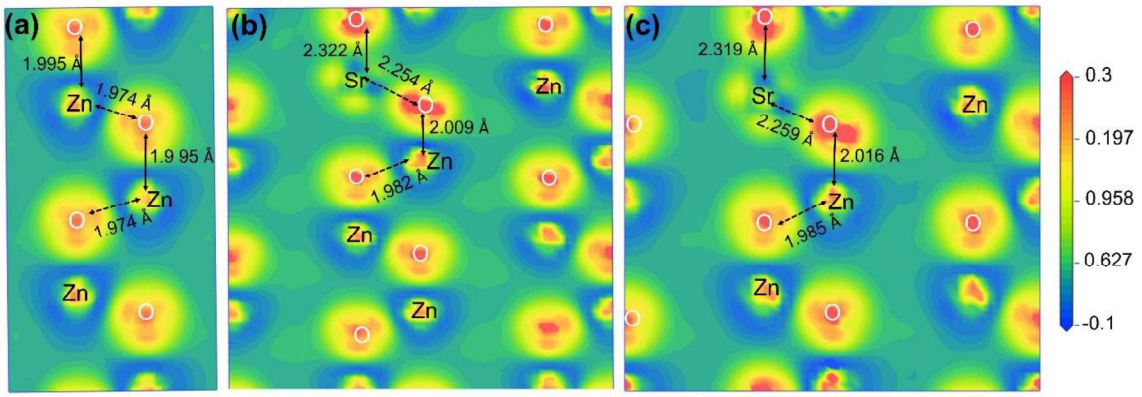

Figure. 7. Calculated charge density contour plot along the (101) plane, (a)- ZnO, (b)- low doping (4.17 at.%; $Zn_{0.9583}Sr_{0.0417}O$) and (c)- high doping (6.25 at.%; $Zn_{0.9375}Sr_{0.0625}O$). In the case of pure and Sr-doped ZnO, the yellow and orange regions surrounding the Zn, O and Sr atom indicate electron enrichment, while the blue and green regions indicate electron loss.

3.3 Optical properties

Based on the previous band structure calculation, we have systematically examined the optical properties of pristine and Sr-doped ZnO based on the complex dielectric function ($\varepsilon(\omega)$), absorption coefficient ($\alpha(\omega)$), reflectivity (R(ω)), and transmittance (T(ω)) by comparing of the optical spectra of pure ZnO. The complex dielectric function is defined as follows:

$$\varepsilon(\omega) = \varepsilon_1 + i\varepsilon_2 \quad (1)$$

In which ω is the incident photon frequency; ε_1 and $\varepsilon_2$are the real and imaginary parts of the dielectric function, respectively. Neglecting the electron correlations, we calculate $\varepsilon_2(\omega)$from the momentum matrix elements between the VB and CB wave function [53]:

$$\varepsilon_2\left(q \to O_{\hat{u},\hbar\omega}\right) = \frac{2\pi e^2}{\Omega\varepsilon_0}\sum_{k,v,c}\langle\Psi_k^c|u.r|\Psi_k^v\rangle^2\delta(E_k^c - E_k^v - E) \quad (2)$$

In this case, e, u, k, Ω, c and v designate respectively the incident photon frequency, the polarization of the incident electric field, the reciprocal lattice vector, the unit cell volume, CB and VB. The values of $\varepsilon_1(\omega)$are calculated from $\varepsilon_2(\omega)$ using the Kramer- Kronig relations [54] owing to the causal response of the dielectric function.

$$\varepsilon_1 = 1 + \frac{2}{\pi}P\int_0^\infty \frac{\varepsilon_2(\omega')\omega'}{\omega'^2 - \omega^2}d\omega \quad (3)$$

Where P is the main value of the integral.

Other optical parameters such as absorption (α (ω)), reflectivity (R (ω)) and transmittance (T (ω)), can be determined respectively using the following relations:

$$\alpha\ (\omega = \frac{\sqrt{2}\omega}{c_0}\left[\sqrt{\varepsilon_1^2(\omega) + \varepsilon_2^2(\omega)} - \varepsilon_1(\omega)\right]^{\frac{1}{2}} (4)$$

$$\mathrm{R}(\omega) = \left|\frac{\sqrt{\varepsilon_1 + \mathrm{i}\varepsilon_2} - 1}{\sqrt{\varepsilon_1 + \mathrm{i}\varepsilon_2} + 1}\right|^2 \quad (5)$$

$$\mathrm{T}(\omega) = (1 - \mathrm{R})^2\mathrm{e}^{-\alpha\mathrm{d}} \quad (6)$$

Where C_0 is the speed of light in vacuum and d is the thickness of the film which equals 250 nm in this study. The interference due to the multiple reflections at the interface between the thin film and the vacuum are neglected in the above formula. We have verified that this does not modify the optical results in the present case.

3.3.1 Dielectric Function

Figure 8 presents the imaginary and real parts of the dielectric function of pure ZnO and SZO systems. We will first investigate the imaginary part of the dielectric function (Figure 8 (a)), in which we clearly observed that there is a significant distinction between the low and high doping in SZO systems. Each peak's location is affected through the values of $U_{d,(Zn)}$ and $U_{p,(O)}$ in several exchange-correlation functions such PBE, which either lower or raise the states included in the transition between the CB and the VB for producing a given peak.

For pure ZnO, Figure 8 (b) shows three distinct peaks in $\varepsilon_2(\omega)$, located at different values of the incident photon energy, which is in good agreement with the experimental results [55] and theoretical calculations [32, 56]. Firstly, the electronic transition from the upper VB (O 2p states) to the lower CB (Zn 4s states), results in the first peak located at 3.3 eV, which is closely related to the band edge emission of ZnO [57]. In addition, both the second and third peaks around 7.5-10.5 eV and 15.25 eV are associated to the electronic transition of O 2p to Zn 3d and Zn 3d to O 2s states in the valence band, respectively. As we can see in Figure 8 (c), for low doping (i.e. 4.17 at.%), the peaks located at high energy regions (12.5-17.5 eV) are shifted to a lower energy state, as well as the energy level of SZO is higher than the intrinsic optical transition of pure ZnO. Within the same context, the SZO has not made any new visible optical transition, which gives rise to an increase in the transmission in the visible region. Moreover, according to the previous DOS analysis (Figure 4 (b)), this peak in the low energy level corresponds to electron excitation of O 2p states from occupied VB to unoccupied CB (Sr 5s states). This process of absorption resulted in a decrease in transmittance in the red and infrared regions.

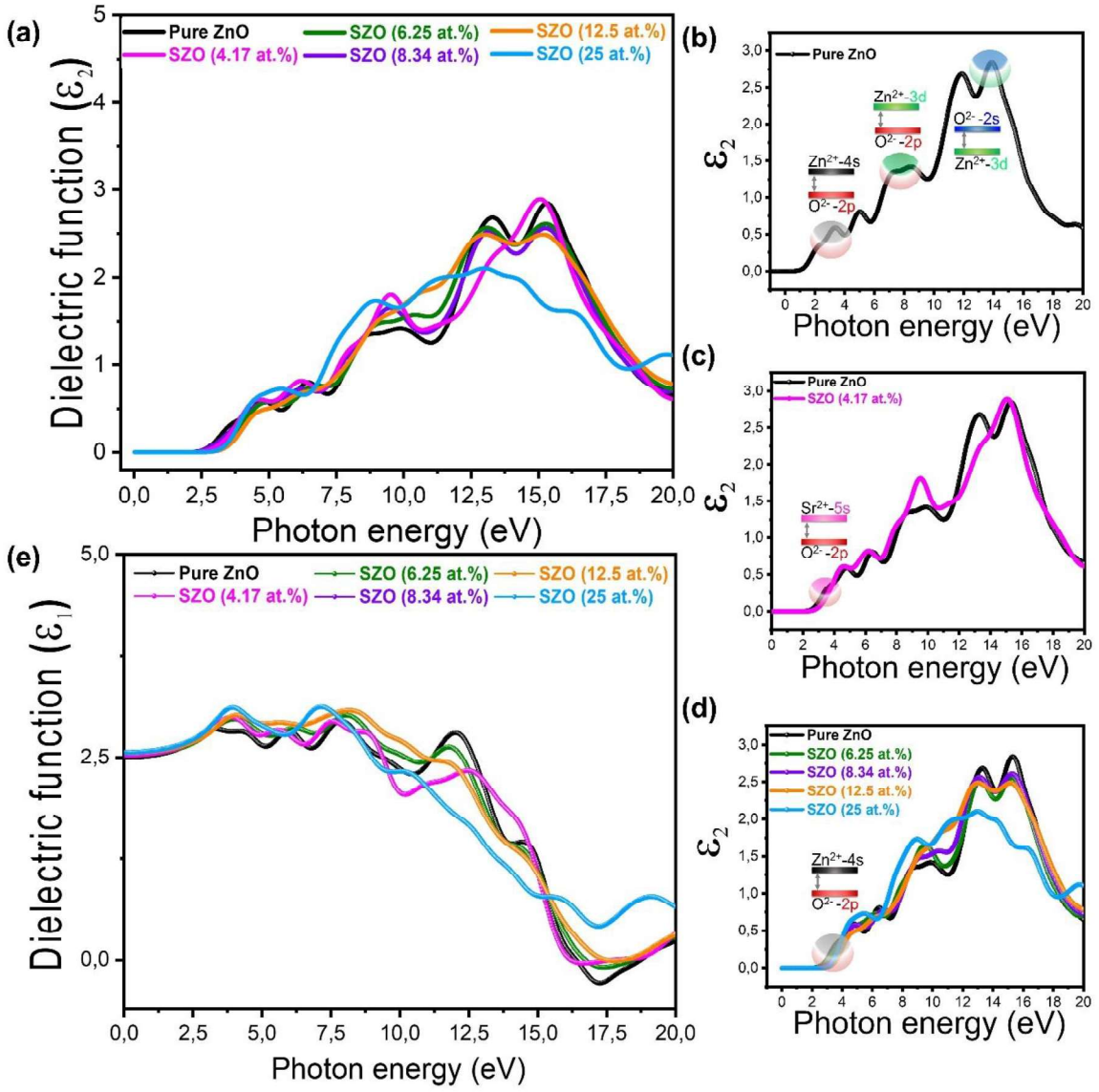

Figure. 8. Imaginary and real parts of the dielectric function for pure ZnO and SZO systems.

Besides, for high doping of SZO (i.e. 6.25, 8.34, 12.5 and 25 at.%), the main peaks around 15.25 eV are significantly weakened and shift to higher energies with increasing Sr concentration (Figure 8 (d)), indicating that the range of absorption frequency narrows and the average optical transmittance increases. In addition, the peaks located in the range of 7.5-10.5 eV become stronger than that of the intrinsic optical transition of ZnO, with increasing Sr concentration, which is due to the strong hybridization between the Zn 3d and O 2p states. Moreover, in low energy level (1.6-3.2 eV), the peaks are enhanced successively with increasing Sr concentration

(Figure 8 (d)). These observed peaks in SZO systems, should be due to the electronic transitions from the upper VB (O 2p states) to the lower CB (Zn 4s states). Similar results were observed for the real part of the dielectric function (Figure 8 (e)), as well as the same energy peak displacement was observed.

3.3.2 Absorption, reflectivity and transmittance

Figure 9 shows the calculated absorption, reflectivity and transmittance spectra for pure ZnO and SZO systems at different values of the incident photon energy. As shown in Figure 9 (a), pure ZnO exhibits the most prominent peak around 16.8 eV (λ =73.8 nm) which is called the vacuum ultraviolet region, indicating that pure ZnO exhibits better absorption in the ultraviolet region. Furthermore, at low Sr concentration (i.e. 4.17 at.%), the reflectivity and transmittance in the red and infrared regions are higher and smaller, respectively, than those of pure ZnO (Figures 9 (b) and (c)). In addition, the spectrum shifted to lower energy regions from 16.8 eV for pure ZnO to 15.74 eV after doping (See inset Figure 9 (a)). This red shift obtained in our work at low Sr concentration is in agreement with the experimental result [20, 23].

In contrast, when the Sr concentration increases from 6.25 to 25 at.%, in the visible light range of 1.6-3.2 eV (λ = 380- 780 nm), the absorption of SZO is lightly increased compared to pure ZnO, resulting in a slight decrease in transmittance in the visible region (Figure 9 (c)). Details regarding the calculated absorption, reflectivity and transmittance spectra for pure ZnO and SZO systems at different values of wavelengths are given in Figure S3. In addition, in the ultraviolet light range of 7.5-12.4 eV, the absorption of SZO systems becomes significantly more pronounced than pure ZnO, improving the absorption behaviour of SZO systems and decreasing the transmittance in the UV region from λ = 100 to 160 nm (Figure S3 (c)). For the highest absorption peak at 16.8 eV (λ =73.8 nm), the absorption of SZO systems becomes significantly weaker than pure ZnO, which significantly decreases the reflectivity in the UV region (Figure 9 (b)). As we can see from the zoom in Figure 9 (a), for high doping, the peak shifts to higher

energy regions from 16.8 eV for pure ZnO to 17.04 eV after doping (i.e. 12.5 at.%). This result is in agreement with that obtained experimentally by Vijayan et al [18]. We observed similar trends in the reflectivity-results (Figure 9 (b)). Indeed, for high doping, in the far ultraviolet range from 12.5 to 20 eV, the reflectivity and transmittance decreases and increases significantly after doping, respectively. Besides, in the energy range of 7.5-12.5 eV and 1.6-3.2 eV, the reflectivity of SZO systems increases markedly after doping (Figure 9 (b)).

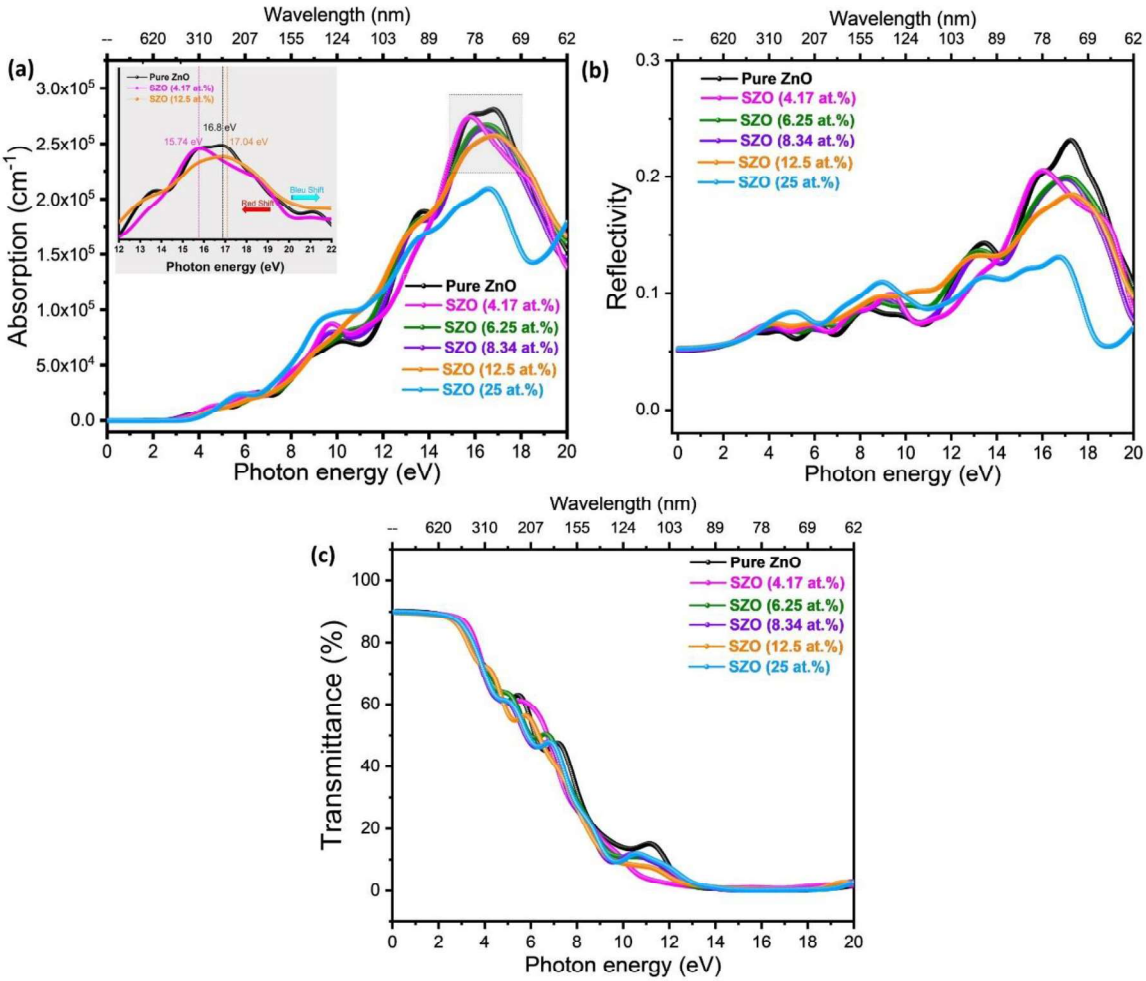

Figure. 9. Optical properties of ZnO and SZO systems: (a), (b) and (c) represent respectively absorption, reflectivity and transmittance at different values of the incident photon energy and wavelengths.

According to Figure S3 (c) (See Supporting Information), the transmittance of pure ZnO is 87% in the visible region (λ =470 nm) and 57 % in the UV region (λ =210 nm). As a result, the transmittance values obtained for low doping (4.17 at.%) in the visible and UV regions were

88.5% and 60%, respectively, which are higher than those of pure ZnO (See inset Figure S3 (c)). We found that the main transmission region of SZO systems is in the range of 250-550 nm, resulting in a high transmittance at low Sr concentrations compared to pure ZnO. While, it relatively decreased slightly due to the increase of absorption in the range of 550-1000 nm compared with pure ZnO (Figure S3 (c)). A similar result was obtained experimentally by Raghavendra et al. [20]. At high concentration of SZO, in the ultraviolet light range of λ = 100-160 nm (See inset Figure S3 (c)), the stronger and broader occupied states result in lower transmission than pure ZnO, which becomes slightly greater in the range of 250-550 nm. Then, it slightly decreased owing to the enhancement of absorption in the range of 550-1000 nm, which relatively increased the absorption coefficient in the visible light region. Hence, the weak and strong doping of ZnO significantly improves the optical performance of SZO systems.

4. Conclusion

In conclusion, this paper provides detailed information on the crystal structure, electronic and optical properties of SZO systems using GGA-PBE+U calculations. Our results highlighted that the difference between lattice parameters and experimental measurements is approximately less than 1%, and that the calculated band gaps for both low and high doping systems are in agreement with the experimental values. The electronic results show that Sr doping is an effective method to adjust its electronic and optical properties, where low Sr concentrations lead to a downward shift in the conduction band, while high Sr concentrations lead to an upward shift in the conduction band, thus increasing the band gap of pure ZnO after doping. Furthermore, the analyses of the optical properties validate the electronic analysis, provide good agreement with the experimental data and improve the optical performance of the SZO systems. Therefore, these results could also serve as a theoretical reference for future research on Sr-doped ZnO and extend the scope of the targeted application.

Acknowledgments

Special thanks to the International Center of Theoretical Physics (ICTP - Trieste-Italy). M.A. thanks N. De Moor for its help for the simulation of the optical response of thin film.

References

[1] R.D. Vispute, V. Talyansky, S. Choopun, R.P. Sharma, T. Venkatesan, M. He, X. Tang, J.B. Halpern, M.G. Spencer, Y.X. Li, L.G. Salamanca-Riba, A.A. Iliadis, K.A. Jones, Heteroepitaxy of ZnO on GaN and its implications for fabrication of hybrid optoelectronic devices, Appl. Phys. Lett. 73 (1998) 348–350. https://doi.org/10.1063/1.121830.

[2] L. Wang, N.C. Giles, Temperature dependence of the free-exciton transition energy in zinc oxide by photoluminescence excitation spectroscopy, J. Appl. Phys. 94 (2003) 973–978. https://doi.org/10.1063/1.1586977.

[3] Ü. Özgür, D. Hofstetter, H. Morkoç, ZnO Devices and Applications: A Review of Current Status and Future Prospects, Proc. IEEE. 98 (2010) 1255–1268. https://doi.org/10.1109/JPROC.2010.2044550.

[4] X. Dai, Z. Zhang, Y. Jin, Y. Niu, H. Cao, X. Liang, L. Chen, J. Wang, X. Peng, Solution-processed, high-performance light-emitting diodes based on quantum dots, Nature. 515 (2014) 96–99. https://doi.org/10.1038/nature13829.

[5] Y. Chen, Review of ZnO Transparent Conducting Oxides for solar applications, IOP Conf. Ser.: Mater. Sci. Eng. 423 (2018) 012170. https://doi.org/10.1088/1757-899X/423/1/012170.

[6] R.L. Hoffman, B.J. Norris, J.F. Wager, ZnO-based transparent thin-film transistors, Appl. Phys. Lett. 82 (2003) 733–735. https://doi.org/10.1063/1.1542677.

[7] N.D. Khoang, H.S. Hong, D.D. Trung, N.V. Duy, N.D. Hoa, D.D. Thinh, N.V. Hieu, On-chip growth of wafer-scale planar-type ZnO nanorod sensors for effective detection of CO gas, Sens. Actuators B Chem. 181 (2013) 529–536. https://doi.org/10.1016/j.snb.2013.02.047.

[8] Y. Kang, F. Yu, L. Zhang, W. Wang, L. Chen, Y. Li, Review of ZnO-based nanomaterials in gas sensors, Solid State Ion. 360 (2021) 115544. https://doi.org/10.1016/j.ssi.2020.115544.

[9] C.A.K. Gouvêa, F. Wypych, S.G. Moraes, N. Durán, N. Nagata, P. Peralta-Zamora, Semiconductor-assisted photocatalytic degradation of reactive dyes in aqueous solution, Chemosphere. 40 (2000) 433–440. https://doi.org/10.1016/S0045-6535(99)00313-6.

[10] W. Yu, J. Zhang, T. Peng, New insight into the enhanced photocatalytic activity of N-, C- and S-doped ZnO photocatalysts, Appl. Catal. B: Environ. 181 (2016) 220–227. https://doi.org/10.1016/j.apcatb.2015.07.031.

[11] C.-Y. Tsay, C.-W. Wu, C.-M. Lei, F.-S. Chen, C.-K. Lin, Microstructural and optical properties of Ga-doped ZnO semiconductor thin films prepared by sol–gel process, Thin Solid Films. 519 (2010) 1516–1520. https://doi.org/10.1016/j.tsf.2010.08.170.

[12] F. Maldonado, A. Stashans, Al-doped ZnO: Electronic, electrical and structural properties, J. Phys. Chem. Solids. 71 (2010) 784–787. https://doi.org/10.1016/j.jpcs.2010.02.001.

[13] T. Srinivasulu, K. Saritha, K.T.R. Reddy, Synthesis and characterization of Fe-doped ZnO thin films deposited by chemical spray pyrolysis, Mod. Electron. Mater. 3 (2017) 76–85. https://doi.org/10.1016/j.moem.2017.07.001.

[14] X.D. Zhang, M.L. Guo, Y.Y. Shen, C.L. Liu, Y.H. Xue, F. Zhu, L.H. Zhang, Electronic structure and optical transition in heavy metal doped ZnO by first-principle calculations, Comput. Mater. Sci. 54 (2012) 75–80. https://doi.org/10.1016/j.commatsci.2011.10.003.

[15] J.-C. Sin, S.-M. Lam, K.-T. Lee, A.R. Mohamed, Preparation and photocatalytic properties of visible light-driven samarium-doped ZnO nanorods, Ceram. Int. 39 (2013) 5833–5843. https://doi.org/10.1016/j.ceramint.2013.01.004.

[16] X. Qiu, G. Li, X. Sun, L. Li, X. Fu, Doping effects of Co^{2+} ions on ZnO nanorods and their photocatalytic properties, Nanotechnology. 19 (2008) 215703. https://doi.org/10.1088/0957-4484/19/21/215703.
[17] W. Water, Y.-S. Yan, Characteristics of strontium-doped ZnO films on love wave filter applications, Thin Solid Films. 515 (2007) 6992–6996. https://doi.org/10.1016/j.tsf.2007.02.028.
[18] T.A. Vijayan, R. Chandramohan, S. Valanarasu, J. Thirumalai, S.P. Subramanian, Comparative investigation on nanocrystal structure, optical, and electrical properties of ZnO and Sr-doped ZnO thin films using chemical bath deposition method, J Mater Sci. 43 (2008) 1776–1782. https://doi.org/10.1007/s10853-007-2404-1.
[19] R. Udayabhaskar, B. Karthikeyan, Role of micro-strain and defects on band-gap, fluorescence in near white light emitting Sr doped ZnO nanorods, J. Appl. Phys. 116 (2014) 094310. https://doi.org/10.1063/1.4893562.
[20] P.V. Raghavendra, J.S. Bhat, N.G. Deshpande, Enhancement of photoluminescence in Sr doped ZnO thin films prepared by spray pyrolysis, Mater. Sci. Semicond. Process. 68 (2017) 262–269. https://doi.org/10.1016/j.mssp.2017.06.028.
[21] A. Ouhaibi, M. Ghamnia, M.A. Dahamni, V. Heresanu, C. Fauquet, D. Tonneau, The effect of strontium doping on structural and morphological properties of ZnO nanofilms synthesized by ultrasonic spray pyrolysis method, J. Sci.: Adv. Mater. Devices. 3 (2018) 29–36. https://doi.org/10.1016/j.jsamd.2018.01.004.
[22] M. Yarahmadi, H. Maleki-Ghaleh, M.E. Mehr, Z. Dargahi, F. Rasouli, M.H. Siadati, Synthesis and characterization of Sr-doped ZnO nanoparticles for photocatalytic applications, J. Alloys Compd. 853 (2021) 157000. https://doi.org/10.1016/j.jallcom.2020.157000.
[23] S. Suwanboon, W. Somraksa, P. Amornpitoksuk, C. Randorn, Effect of trisodium citrate on the formation and structural, optical and photocatalytic properties of Sr-doped ZnO, J. Alloys Compd. 832 (2020) 154963. https://doi.org/10.1016/j.jallcom.2020.154963.
[24] Y. Pan, Effects of Cu, Ag and Au on electronic and optical properties of α-Ga_2O_3 oxide according to first-principles calculations, J. Phys. Chem. Solids. 174 (2023) 111152. https://doi.org/10.1016/j.jpcs.2022.111152.
[25] K. Harun, N.A. Salleh, B. Deghfel, M.K. Yaakob, A.A. Mohamad, DFT + U calculations for electronic, structural, and optical properties of ZnO wurtzite structure: A review, Results Phys. 16 (2020) 102829. https://doi.org/10.1016/j.rinp.2019.102829.
[26] M. Achehboune, M. Khenfouch, I. Boukhoubza, I. Derkaoui, B.M. Mothudi, I. Zorkani, A. Jorio, Effect of Yb concentration on the structural, magnetic and optoelectronic properties of Yb doped ZnO: first principles calculation, Opt Quant Electron. 53 (2021) 709. https://doi.org/10.1007/s11082-021-03369-x.
[27] Y. Pan, First-principles investigation of structural stability, electronic and optical properties of suboxide (Zr_3O), Mater. Sci. Eng. B. 281 (2022) 115746. https://doi.org/10.1016/j.mseb.2022.115746.
[28] Y. Pan, First-principles investigation of the effect of noble metals on the electronic and optical properties of GaN nitride, Mater. Sci. Semicond. Process. 151 (2022) 107051. https://doi.org/10.1016/j.mssp.2022.107051.
[29] M. Achehboune, M. Khenfouch, I. Boukhoubza, I. Derkaoui, L. Leontie, A. Carlescu, B.M. Mothudi, I. Zorkani, A. Jorio, Optimization of the luminescence and structural properties of Er-doped ZnO nanostructures: effect of dopant concentration and excitation wavelength, J. Lumin. 246 (2022) 118843. https://doi.org/10.1016/j.jlumin.2022.118843.
[30] P. Makkar, N.N. Ghosh, A review on the use of DFT for the prediction of the properties of nanomaterials, RSC Adv. 11 (2021) 27897–27924. https://doi.org/10.1039/D1RA04876G.

[31] Y. Pan, J.L. Chen, M. Wen, W.M. Guan, First-principles investigation of structural, mechanical and thermodynamic properties of NiPt2 bimetallic nanomaterial, Chem. Phys. Lett. 719 (2019) 34–38. https://doi.org/10.1016/j.cplett.2019.01.045.
[32] M. Achehboune, M. Khenfouch, I. Boukhoubza, I. Derkaoui, B.M. Mothudi, I. Zorkani, A. Jorio, A DFT study on the electronic structure, magnetic and optical properties of Er doped ZnO: Effect of Er concentration and native defects, Comput. Condens. Matter. 31 (2022) e00627. https://doi.org/10.1016/j.cocom.2021.e00627.
[33] Y. Pan, First- principles investigation of the influence of point defect on the electronic and optical properties of α-Ga_2O_3, Intl J of Energy Research. 46 (2022) 13070–13078. https://doi.org/10.1002/er.8047.
[34] S.J. Clark, M.D. Segall, C.J. Pickard, P.J. Hasnip, M.I.J. Probert, K. Refson, M.C. Payne, First principles methods using CASTEP, Z. fur Krist. - Cryst. Mater. 220 (2005) 567–570. https://doi.org/10.1524/zkri.220.5.567.65075.
[35] J.P. Perdew, K. Burke, M. Ernzerhof, Generalized Gradient Approximation Made Simple, Phys. Rev. Lett. 77 (1996) 3865–3868. https://doi.org/10.1103/PhysRevLett.77.3865.
[36] D. Vanderbilt, Soft self-consistent pseudopotentials in a generalized eigenvalue formalism, Phys. Rev. B. 41 (1990) 7892–7895. https://doi.org/10.1103/PhysRevB.41.7892.
[37] L. Qiao, C. Chai, Y. Yang, X. Yu, C. Shi, First-principles theoretical study on band of strained wurtzite Nb-doped ZnO, J. Wuhan Univ. Technol.-Mat. Sci. Edit. 30 (2015) 467–472. https://doi.org/10.1007/s11595-015-1173-y.
[38] H.J. Monkhorst, J.D. Pack, Special points for Brillouin-zone integrations, Phys. Rev. B. 13 (1976) 5188–5192. https://doi.org/10.1103/PhysRevB.13.5188.
[39] Z. Xu, Q. Hou, F. Guo, Y. Li, Y. Liu, Effect of strains on the optical and magnetic properties of Ce-doped ZnO with O or Zn vacancies, J Mater Sci. 55 (2020) 7390–7402. https://doi.org/10.1007/s10853-020-04551-4.
[40] H.-C. Wu, Y.-C. Peng, C.-C. Chen, Effects of Ga concentration on electronic and optical properties of Ga-doped ZnO from first principles calculations, Opt. Mater. 35 (2013) 509–515. https://doi.org/10.1016/j.optmat.2012.10.022.
[41] X. Ma, B. Lu, D. Li, R. Shi, C. Pan, Y. Zhu, Origin of Photocatalytic Activation of Silver Orthophosphate from First-Principles, J. Phys. Chem. C. 115 (2011) 4680–4687. https://doi.org/10.1021/jp111167u.
[42] I. Derkaoui, M. Achehboune, I. Boukhoubza, Z. El Adnani, A. Rezzouk, Improved first-principles electronic band structure for cubic ($Pm\bar{3}m$) and tetragonal (P4mm, P4/mmm) phases of $BaTiO_3$ using the Hubbard U correction, Comput. Mater. Sci. 217 (2023) 111913. https://doi.org/10.1016/j.commatsci.2022.111913.
[43] D. Issam, M. Achehboune, I. Boukhoubza, R. Hatel, Z. El Adnani, A. Rezzouk, Investigation of the Crystal Structure, Electronic and Optical Properties of Cr-Doped $BaTiO_3$ on the Ti Site Using First Principles Calculations. J Phys Chem Solids. 175 (2023), 111209, https://doi.org/10.1016/j.jpcs.2022.111209.
[44] W. Ranke, Separation of the partial s- and p-densities of valence states of ZnO from UPS-measurements, Solid State Commun. 19 (1976) 685–688. https://doi.org/10.1016/0038-1098(76)91105-4.
[45] A. Mahmood, F. Tezcan, G. Kardaş, F. Karadağ, Effect of Sr doping on the electronic band structure and optical properties of ZnO: A first principle calculation, J. Appl. Phys. 122 (2017) 113102. https://doi.org/10.1063/1.5002075.
[46] B.E. Sernelius, K.-F. Berggren, Z.-C. Jin, I. Hamberg, C.G. Granqvist, Band-gap tailoring of ZnO by means of heavy Al doping, Phys. Rev. B. 37 (1988) 10244–10248. https://doi.org/10.1103/PhysRevB.37.10244.

[47] E. Yu, Y. Pan, Catalytic properties of borophene/MoS $_2$ heterojunctions for hydrogen evolution reaction under different stacking conditions, J. Mater. Chem. A. 10 (2022) 24866–24876. https://doi.org/10.1039/D2TA05928B.
[48] E. Yu, Y. Pan, Exploring the hydrogen evolution catalytic activity of the orthorhombic and hexagonal borophene as the hydrogen storage material, Electrochimica Acta. 435 (2022) 141391. https://doi.org/10.1016/j.electacta.2022.141391.
[49] S. Chen, Y. Pan, Mechanism of interlayer spacing on catalytic properties of MoS_2 from ab-initio calculation, Appl. Surf. Sci. 599 (2022) 154041. https://doi.org/10.1016/j.apsusc.2022.154041.
[50] Y. Pan, E. Yu, Theoretical prediction of structure, electronic and optical properties of VH2 hydrogen storage material, Int. J. Hydrog. Energy. 47 (2022) 27608–27616. https://doi.org/10.1016/j.ijhydene.2022.06.080.
[51] Y. Pan, H.W. Huang, W.M. Guan, First-principles investigation of structural stability, mechanical properties and electronic structure of $Ru_{1-x}Re_xB_2$ and $Re_{1-x}Ru_xB_2$ borides, Comput. Mater. Sci. 89 (2014) 19–23. https://doi.org/10.1016/j.commatsci.2014.03.029.
[52] Y. Pan, Structural, elastic properties and electronic structure of Cr_3B_4 -type borides: An ultra-incompressible material, Comput. Mater. Sci. 92 (2014) 57–62. https://doi.org/10.1016/j.commatsci.2014.05.031.
[53] R. Chowdhury, S. Adhikari, P. Rees, Optical properties of silicon doped ZnO, Physica B: Condens. Matter. 405 (2010) 4763–4767. https://doi.org/10.1016/j.physb.2010.08.072.
[54] L. Li, W. Wang, H. Liu, X. Liu, Q. Song, S. Ren, First Principles Calculations of Electronic Band Structure and Optical Properties of Cr-Doped ZnO, J. Phys. Chem. C. 113 (2009) 8460–8464. https://doi.org/10.1021/jp811507r.
[55] R.L. Hengehold, R.J. Almassy, F.L. Pedrotti, Electron Energy-Loss and Ultraviolet-Reflectivity Spectra of Crystalline ZnO, Phys. Rev. B. 1 (1970) 4784–4791. https://doi.org/10.1103/PhysRevB.1.4784.
[56] Y.-S. Lee, Y.-C. Peng, J.-H. Lu, Y.-R. Zhu, H.-C. Wu, Electronic and optical properties of Ga-doped ZnO, Thin Solid Films. 570 (2014) 464–470. https://doi.org/10.1016/j.tsf.2014.04.037.
[57] L. Duan, B. Lin, W. Zhang, S. Zhong, Z. Fu, Enhancement of ultraviolet emissions from ZnO films by Ag doping, Appl. Phys. Lett. 88 (2006) 232110. https://doi.org/10.1063/1.2211053.